García Ivars, J.; Iborra Clar, MI.; Alcaina Miranda, MI.; Van Der Bruggen, B. (2015). Comparison between hydrophilic and hydrophobic metal nanoparticles on the phase separation phenomena during formation of asymmetric polyethersulphone membranes. Journal of Membrane Science. 493:709-722. doi:10.1016/j.memsci.2015.07.009.

Comparison between hydrophilic and hydrophobic metal nanoparticles on the phase separation phenomena during formation of asymmetric polyethersulphone membranes

Jorge Garcia-Ivars*[a], Maria-Isabel Iborra-Clar[a,b], Maria-Isabel Alcaina-Miranda[a,b], Bart Van der Bruggen[c]

[a] Research Institute for Industrial, Radiophysical and Environmental Safety (ISIRYM), Universitat Politècnica de València, C/Camino de Vera s/n, 46022 Valencia, Spain

[b] Department of Chemical and Nuclear Engineering, Universitat Politècnica de València, C/Camino de Vera s/n, 46022 Valencia, Spain

[c] Department of Chemical Engineering, KU Leuven, Willem de Croylaan 46, B-3001 Heverlee, Belgium

Tel. +34 963879633

Fax. +34 963877639

Correspondence to: Jorge Garcia-Ivars (E-mail: *jorgariv@posgrado.upv.es*)

ABSTRACT

Inorganic nanoparticles have been applied as additive in membrane synthesis for improving different properties from the base polymer such as hydrophilicity, fouling resistance or permselectivity. To investigate the changes caused by the presence of the inorganic nanoparticles in the formation of the membrane structure, two different metallic compounds with opposite hydrophilicity were used as additives: hydrophilic zinc oxide (ZnO) and hydrophobic tungsten disulphide (WS_2). For this purpose, the effect of these metal nanoparticles at ultra-low concentrations (0.05 and 0.25 wt% metal nanoparticles/polymer ratio) in the preparation of flat-sheet membranes based on polyethersulphone (PES) by immersion-precipitation method was investigated. N-methyl-2-pyrrolidone (NMP) was used as solvent. The influence of both metal

nanoparticles on the characteristics and permselective properties of PES membranes was studied with microscopic observations, contact angle measurements, and filtration experiments. Although the incorporation of metal nanoparticles could turn the system into thermodynamically unstable, the demixing process during formation of membranes was slightly delayed, suppressing the macrovoid formation (remarkably using WS_2). Regardless the nature of the metal nanoparticles, results showed an overall improvement in membrane hydrophilicity and permselectivity by adding metal nanoparticles compared to the control PES membrane, demonstrating that the behaviour of both metal nanoparticles at ultra-low concentrations was very similar.

KEYWORDS membrane synthesis; hydrophilicity; phase inversion; metal nanoparticles; filtration experiments.

1. INTRODUCTION

Non-solvent induced phase separation method (NIPS) is the most widely used technique to prepare membranes with different morphologies and properties varying from microfiltration to pervaporation and gas separation [1]. This process is governed by the thermodynamic and diffusional properties of the different components present in the system, which is usually composed of a polymer, a solvent and a non-solvent. Thermodynamic properties are usually studied by the ternary phase diagram formed by the previous components, where the construction of the cloud point curve can be used to obtain the binodal curve of liquid-liquid phase separation, which determines the membrane structure. In this way, the composition at which the polymer solution (basically formed by at least one polymer dissolved in at least one solvent) is no longer thermodynamically stable can be determined [2]. However, besides thermodynamics,

the kinetics factors (such as diffusion rate) also play an important role in the morphology development. When the polymer solution (or dope solution) is immersed in a non-solvent bath (or coagulation bath), polymer is solidified through the exchange between the solvent and non-solvent [3]. In their studies, Reuvers et al. predicted two types of demixing in a membrane forming-system using the Flory-Huggins theory with binary data on thermodynamics and on the diffusional behaviour of the components present in the system: delayed and instantaneous demixing [4,5]. Different authors demonstrated that the formation of porous substructures with open and large channel-like cavities (called macrovoids) is related to the mechanism of instantaneous demixing [6-8]. In the same way, slow precipitation rates (delayed demixing) produce sponge-like structures [3,9]. For these reasons, the choice of solvent/non-solvent system (related to their miscibility), the composition of polymer solution, the composition of the coagulation bath and the casting conditions are key factors during membrane preparation process [10].

The comprehension of the different processes taking place in the ternary system is essential to understand the membrane formation mechanism. However, this system is never used neither in commercial applications nor in research field. The presence of additives in the polymer/solvent/non-solvent system (forming a quaternary or pseudo-ternary system) could be very important to control the membrane morphology and to improve some characteristics of the nascent membrane such as mechanical, thermal, magnetic, hydrophilic and even antifouling properties. The incorporation of additives in the casting solution (blending modification) or in the coagulation bath has been studied in a micro or nanoscale by many researchers [11-13].

Nanotechnology involves the creation, modification and use of both materials and systems at a size scale lower than 100 nm. The aim of this technology is its ability to be developed in a wide range of purposes, regardless of the research field. Examples of some applications of nanotechnology are: to treat the oxidative states and to prevent scarring after glaucoma surgery in ophthalmology [14], as nanocarriers to treat cancer or malaria [15], to improve lithium battery systems [16], in food structure research [17], and in membrane separation processes. In the last case, the nanotechnology applied to membrane synthesis has recently caught the attention of many researchers in order to combine the unique properties of the nanoscale structures (such as catalytic activity and antimicrobial) with the morphology and polymer properties to prepare mixed matrix membranes (MMMs), which can be defined as inorganic and organic nanofillers dispersed at a nanometer level in a polymer matrix [18]. These membranes may also be referred to as "hybrid inorganic-organic nanocomposite membranes". MMMs make use of the benefits of the transport properties of both inorganic and organic materials in the polymer matrix that provide higher strength, permselectivity and antifouling characteristics compared to bare polymeric membranes. Some examples are polymeric membranes modified with zeolite [19], zero-valent metals [20], carbon nanotubes [21], metal oxide nanoparticles [22], and fullerenes [23].

Normally, the studies about membrane modification using metal nanoparticles as additives are focused on their hydrophilic or hydrophobic character rather than the synergism caused by their own presence in the matrix structure and on the membrane surface, regardless of their hydrophobicity. No papers have reported the effect of ultra-low concentrations of metal nanoparticles with different nature and hydrophobicity on membrane morphology. For this reason, in order to explore the changes caused by the

presence of the inorganic nanoparticles even at ultra-low concentrations on the formation of the membrane structure, the novelty of the present work is to investigate the effect of two inorganic compounds with different physical and chemical characteristics and opposite hydrophobicity in the formation of membranes made of polyethersulphone (PES) by phase inversion method (NIPS in this case): a well-known hydrophilic metal oxide (zinc oxide, ZnO) and a hydrophobic transition metal chalcogenide (tungsten disulphide, WS_2). Both metal nanoparticles are widely used as additives in both research and commercial applications due to their unique structure and functional properties, which are different from those of the bulk forms. Similar to other metal oxides in nanoparticle form (such as TiO_2), nano-sized ZnO show excellent antibacterial, antifungal and anticorrosion features, including promising catalytic activity, high surface area, photosensitivity, chemical stability, hydrophilicity, and low cost compared to TiO_2 and Al_2O_3. For these reasons, ZnO nanoparticles have been used by other researchers as additive in blending modification of polymer membranes for improving hydrophilic and antifouling properties [24,25]. As transition metal chalcogenide (such as MoS_2), nano-sized WS_2 is insoluble in common solvents and practically inert and has some interesting electronic and optical properties. Due to their hydrophobic character, WS_2 nanoparticles can be used as additives to increase the hydrophobicity of polymer films (such as polytetrafluoroethylene) and as a photocatalyst, especially when these nanoparticles are coupled to TiO_2 and SiO_2 for organic matter degradation [26-28].

In this work, morphology, surface properties and composition of each membrane were analysed using Scanning Electron Microscope (SEM), Atomic Force Microscopy (AFM), Energy Dispersive X-ray spectroscopy (EDX), Fourier Transform IR

spectroscopy with Attenuated Total Reflectance (FTIR-ATR), membrane porosity, pore size, and water contact angle measurements. Also, the influence of both compounds on the permeation properties was studied by water permeation, molecular weight cut-off (MWCO) determination and humic acid rejection.

2. EXPERIMENTAL

2.1. Materials

Polyethersulphone (PES, Veradel P 3100, M_W = 35000 Da, supplied by Solvay Advanced Polymer, Belgium) was employed as base polymer and N-methyl-2-pyrrolidone (NMP, purity of 99.5 %, purchased from Sigma Aldrich, Germany) was selected as solvent and used without further purification. The non-woven support was commercial grade Viledon FO 2471 from Freudenberg (Germany). WS_2 and ZnO were used as additives in nanoparticle form, where the former was supplied by MK nano, MK Impex Corp. (Canada) and the latter was purchased from Sigma Aldrich (Germany) with a particle size lower than 50 nm. Polyethylene glycols (PEGs) of different molecular weights (from 6000 to 20000 Da) were selected for MWCO characterisation. Humic Acid (HA) was used as feed solution to during fouling experiments because this compound is one of the main well-known foulant and also the main component for natural organic matter (NOM) in surface waters, causing different adverse effects such as the growth of microbial population, unpleasant odours, changes in colour, and the formation of different dangerous by-products for human health (trihalomethanes or haloacetic acids) [29,30]. Both solutes (PEG and HA) were also purchased from Sigma Aldrich (Germany). All reagents were employed as received without further purification. Deionised water was used throughout this study.

2.2. Membrane preparation

Membranes were prepared by using non-solvent induced phase separation method (NIPS). Firstly, different additive concentrations (i.e. 0.05 and 0.25 wt% metal nanoparticles/PES ratio) were fully dispersed in NMP for 3 h by vigorous mechanical stirring (600 rpm) at room temperature (20 ºC). Subsequently, a predetermined amount of PES (20 wt%) was gradually added with continuous stirring at the same conditions for at least 48 h until the polymer was completely dissolved. The polymer concentration used in this study was selected according to previous studies about preparation and modification of polymeric membranes [12,31], whereas these additive concentrations were selected to examine the effect of ultra-low concentrations of metal nanoparticles on the membrane morphology and performance. After obtaining a homogeneous solution, the air bubbles that might be trapped in the polymer solution were removed by vacuum pump (40 ºC for 15 min). Polymer solutions were then cast onto nonwoven supports by using a film applicator (K4340 Automatic Film Applicator, Elcometer) with a 200 μm casting knife at 20 ºC and constant relative humidity (~ 20 %), followed by immediate immersion in a non-solvent coagulation bath (distilled water at 20 ºC) for precipitation. This procedure (the control of both temperature and relative humidity and also the immediate immersion) was implemented to control a preceding dry phase-inversion in the atmosphere. After 1 h, the resulting membranes were washed with deionised water to remove the remaining solvent and finally stored in ultrapure water for further testing. For each composition, three polymer solutions were prepared; obtaining three membranes for each polymer solution.

2.3. Ternary phase diagram for polymer/solvent/non-solvent system

Ternary phase diagram for PES/NMP/water system was constructed by titration method to obtain the clouds points [32]. For this purpose, 5 g of a homogeneous PES/NMP solution prepared with 20 wt% PES was introduced in a sealed container with a magnetic stirrer. Subsequently, a known quantity of water/solvent solution was added dropwise while the PES/NMP solution is thoroughly stirred. When this solution became turbid and persisted during a few minutes (~ 10-15 min), the cloud point was reached. Solvent was then added to dilute the solution and make it clear again. After each change in the composition of the PES/NMP solution, the container weight was recorded to obtain each fraction of the different compounds used.

The same procedure was applied for plotting the ternary phase diagrams for PES + metal nanoparticles/NMP/water systems. The main difference was the presence of different concentrations of additives (0.05 and 0.25 wt% metal nanoparticles/PES ratio) during the preparation of PES/NMP solution in the first stage of this procedure. These solutions were prepared as it was described before (Section 2.2).

2.4. Morphological characterisation

All the synthesised membranes were characterised in terms of water contact angle, membrane porosity, plane and thickness shrinkage ratio, FTIR-ATR, SEM, EDX, and AFM techniques. For this purpose, three samples of each membrane were used for testing.

A contact angle measuring system DSA10 MK2 (Krüss, Germany) was used for determining the water contact angle of each membrane surface. A water droplet (2 ml) was placed on a dry flat homogeneous membrane sample and the contact angle between

the droplet and membrane was measured. The average contact angle for ultrapure water was determined in a series of ten measurements for each membrane sample.

Membrane porosity (ε) of each membrane was determined by wet-dry weighting method, where wet samples were weighed after mopping superficial water and after that, these samples were dried by putting them in a vacuum oven for 24 h at 50 ºC and then they were weighed in a dry state. Therefore, ε was calculated using the following equation [33, 34]:

$$\varepsilon(\%) = \frac{\dfrac{(W_W - W_D)}{\rho_W}}{\dfrac{(W_W - W_D)}{\rho_W} + \dfrac{W_D}{\rho_p}} \cdot 100 \qquad \text{Eq. (1)}$$

where W_W and W_D are the weights of membrane in swollen and dry states, respectively. ρ_W denotes the density of pure water at operating conditions (g/cm^3) and ρ_p represents the density of the polymer (g/cm^3). The overall porosity value was obtained as the average of five different samples of each membrane.

In the same way, shrinkage ratios of all the synthesised membranes were determined using the length (a), width (b) and thickness (h) of each sample considering the theoretical dimensions values before and after the phase inversion process. The theoretical membrane thickness was 380 μm (200 μm from casting knife and 180 μm from non-woven support) and the sample dimensions were 1 x 1 cm. The shrinkage ratio was calculated using the following expressions:

$$ab_{shrinkage}(\%) = \left(1 - \frac{a_{after} \cdot b_{after}}{a_{theoretical} \cdot b_{theoretical}}\right) \cdot 100 \qquad \text{Eq. (2)}$$

$$h_{shrinkage}(\%) = \left(1 - \frac{h_{after}}{h_{theoretical}}\right) \cdot 100 \qquad \text{Eq. (3)}$$

where $ab_{shrinkage}$ is the plane shrinkage ratio (%) and $h_{shrinkage}$ is the thickness shrinkage ratio.

FTIR-ATR spectra of the synthesised membranes were recorded on a Perkin-Elmer Spectrum 100 spectrometer equipped with an ATR accessory in the range from 4000 to 650 cm^{-1}. Membrane samples were dried at the same conditions (by using a vacuum oven at 50 ºC) before the FTIR-ATR analyses.

Cross-sections of the synthesised membranes were observed by scanning electron microscopy (SEM). SEM images were made with a JEOL JSM6300 (Japan) instrument equipped with an adjunct EDX spectrometer in high vacuum condition at an accelerating voltage of 20 keV. Prior to SEM analysis, cross-sections were prepared by fracturing dry membrane samples in liquid nitrogen. These samples were sputtered with a thin conductive layer (< 10 nm) of gold/palladium. In addition, EDX analysis was used to investigate the real composition on the membrane surface. Each reported element composition value was expressed by the average of three measurements for each sample.

The surface AFM images were visualised using a multimode AFM (VEECO Instruments, United States) by a tapping mode. The surface AFM images were obtained in different square areas of each membrane sample based on a scan size of 5 µm x 5 µm. The surface roughness parameters were determined in terms of average roughness (S_a) and the root mean square of the Z data (S_q) by averaging the values measured over a scan area of 1 µm x 1 µm in ten different areas selected arbitrarily for each membrane

sample. Both parameters were calculated by the following expression, considering 512 data points as N_p parameter:

$$S_a = \frac{1}{N_p}\sum_{i=0}^{N}\left|Z_i - Z_{avg}\right| \quad \text{Eq. (4)}$$

$$S_q = \sqrt{\frac{1}{N_p}\sum_{i=0}^{N}\left|Z_i - Z_{avg}\right|^2} \quad \text{Eq. (5)}$$

where Z_i is the current Z value measured, while Z_{avg} is the average of the Z values within the given area and N_p is the number of points within the given area.

2.5. Filtration experiments

The permeation properties of all the prepared membranes were characterised in terms of water permeability (membrane intrinsic resistance), MWCO determination and HA rejection studies using dead-end filtration experiments. For this purpose, three samples of each membrane were used for testing the permselective properties. Firstly, all the membranes were compacted at room temperature and 4 bar in dead-end mode with a Sterlitech HP 4750 stirred cell, with a similar experimental setup as that is shown in [35]. The effective membrane area in the cell was 14.6 cm^2 and its volume capacity was 300 ml. After the compaction procedure, water permeability experiments were carried out with ultrapure water at different operating pressures ranging from 1 to 4 bar at 25 ºC. The ultrapure water flux (J_W, $L/m^2 \cdot h$) was measured using the gravimetric method and was determined by:

$$J_W = \frac{V}{A_m \cdot t} \quad \text{Eq. (6)}$$

where V is the volume of permeate water (m^3), A_m is the effective area of the membrane (m^2) and t is the permeation time (h). The slope of the linear regression of J_W on ΔP was

determined as the water permeability (K_W), which was calculated using the following expression:

$$K_W = \frac{J_W}{\Delta P} \quad \text{Eq. (7)}$$

According to Darcy's law, the membrane intrinsic resistance (R_m) was obtained by Eq. (8):

$$R_m = \frac{1}{\mu \cdot K_W} \quad \text{Eq. (8)}$$

Pore size and MWCO determination of the different synthesised membranes were characterised by solute rejection via ultrafiltration experiments. Aqueous solutions of PEG (1000 ppm) with different molecular weights from 6 to 20 kDa were individually prepared using ultrapure water and used as feed solutions in the above-mentioned filtration setup. The PEG concentration was selected according to previous studies about MWCO determination [36,37]. After compacting each membrane at 4 bar, experiments were carried out at different ΔP ranging from 1 to 4 bar. The effect of the concentration polarisation phenomenon was minimised by using a Teflon coated magnetic stirring bar on the top of the membrane during MWCO determination and fouling experiments [38]. Regression factors obtained for calibrations within the experimental concentration range were above 0.99. PEG rejections were measured by the solute concentration using a Hach Lange IL550 TOC-TN analyser, and were calculated by Eq. (9):

$$R(\%) = \left(1 - \frac{C_p}{C_f}\right) \cdot 100 \quad \text{Eq. (9)}$$

where C_p is the solute concentration in the permeate stream and C_f is the solute concentration in the feed solution.

The solute radius can be obtained from its diffusivity in a solution by using the Stokes-Einstein equation. Details of these calculations were reported by [39]. If it is assumed that the diffusing solute could be a sphere moving in a continuous fluid of solvent, the diffusivity D_{AB} can be expressed as:

$$D_{AB} = \frac{k \cdot T}{6 \cdot \pi \cdot \eta \cdot r} \qquad \text{Eq. (10)}$$

where k is Boltzmann's constant, T is the temperature, η is the solvent viscosity, and r is the hydrodynamic radius or Stokes-Einstein radius. This is known as the Stokes-Einstein equation and is a good approximation for large solutes greater than 0.5 nm [40]. The hydrodynamic radius can be defined as the radius of a hypothetical sphere that diffuses at the same rate as the particle under study.

In the same way, the diffusivity can be determined using the following equation:

$$D_{AB} = \frac{2.5 \cdot 10^{6} kT}{\eta \cdot (M_w [\eta])^{1/3}} \qquad \text{Eq. (11)}$$

where $[\eta]$ is the intrinsic polymer viscosity and M_w is the molecular weight of the solute. If both expressions are combined, the next equation is obtained:

$$r(cm) = 2.122 \cdot 10^{-8} \cdot (M_w [\eta])^{1/3} \qquad \text{Eq. (12)}$$

The intrinsic viscosity of PEG is related to its own molecular weight and it can be calculated using the following equation [41]:

$$[\eta] = 4.9 \cdot 10^{-4} \cdot (M_w)^{0.672} \qquad \text{Eq. (13)}$$

By substituting Eq. (13) in Eq. (12), Stokes-Einstein radii of PEG molecules can be calculated based on their molecular weights:

$$r(cm) = 16.73 \cdot 10^{-10} \cdot M_w^{0.557} \quad \text{Eq. (14)}$$

where r was the Stokes-Einstein radius of PEG in cm, and M_w is the average molecular weight of PEG in g/mol. Therefore, the average pore size can be predicted by the r calculated from the MWCO of the membrane that was determined from the Stokes-Einstein radius of the solute which gives 90 % separation applying this equation. This relationship was extensively used by other researchers [36,42].

After obtaining the MWCO and the water permeation experiments, each synthesised membrane was firstly subjected to a compaction test with ultrapure water at 2 bar during 30 min. Then, a HA solution with concentration of 500 ppm at pH=7 was prepared in ultrapure water by adding 1 mM NaOH (Merck, Germany) solution using a pH meter (Orion pH meter model 420A). This solution was filtered at 2 bar for 1.5 h and the permeate flux during HA filtration J_f (L/m^2·h) was measured by weighing the collected permeates. In order to evaluate the antifouling ability of the membranes tested, normalised flux ratio (*NFR*) was determined by:

$$NFR(\%) = \left(\frac{J_{f2}}{J_{f1}} \right) \cdot 100 \quad \text{Eq. (15)}$$

where J_{f1} and J_{f2} are the permeate fluxes at the beginning and after the fouling filtration, respectively.

Finally, HA rejection for each membrane was calculated by obtaining the HA concentration in the permeate stream using a Shimadzu UV-1601 double beam spectrophotometer (Japan) and applying the Eq. (9).

3. RESULTS AND DISCUSSION

3.1. Morphological study

In order to visualise the effect of the metal nanoparticles in the membrane structure, SEM analysis of the different synthesised membranes was carried out to study the surface and especially cross-sectional morphology in a qualitative way. Fig. 1 presents the SEM images of the cross-sections obtained for each synthesised PES membrane prepared with and without metal nanoparticles in its polymer structure. It can be seen that control PES membrane have an asymmetric structure consisting of a dense thin skin layer on a porous thick open channel-like sublayer with the presence of macrovoids inside the channel-like pores and near to the bottom of the membrane and a skin layer with a dense nodular like structure, which agrees with the typical structure obtained for membranes formed by immersion-precipitation phase inversion method [43]. In general, phase-inversion method is dominated by the exchange rate or affinity between the solvent in the casting solution and the non-solvent in the coagulation bath. The presence of macrovoids indicates that there is a good miscibility between NMP (as solvent) and water (as non-solvent), which allows the penetration of the water into the casting solution (instantaneous demixing) and generates a porous structure [6,44].

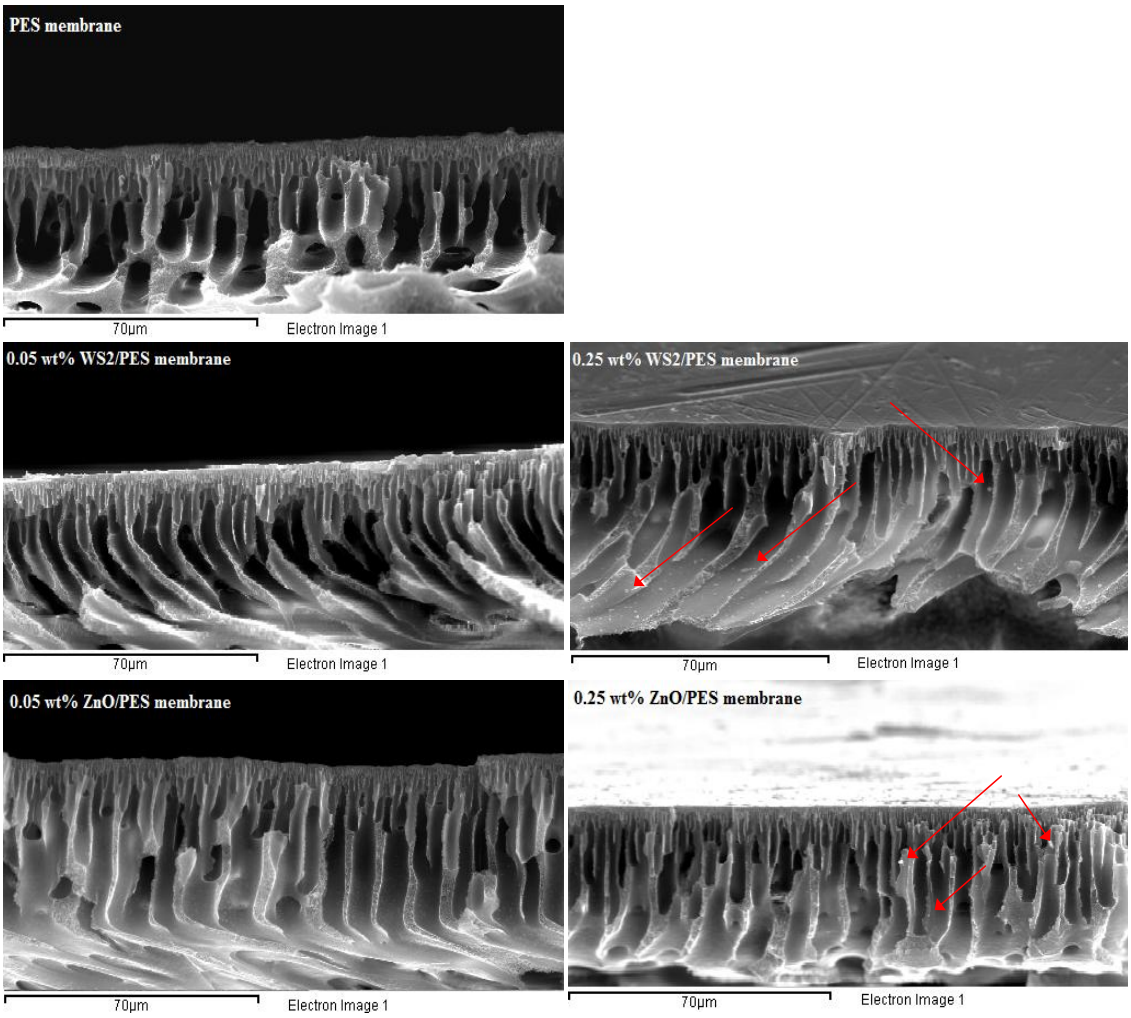

Fig. 1. SEM images of the cross-sections of the synthesised membranes at different concentrations of metal nanoparticles (0, 0.05 and 0.25 wt% metal nanoparticle/PES ratio).

Even at ultra-low concentrations, the incorporation of metal nanoparticles had influence in both thermodynamic and kinetic properties of the PES/NMP/water system, resulting in interesting modifications in the inner membrane structure: the open channel-like structure with macrovoids turn into a longer and narrower finger-like structure with partial or total suppression of macrovoids. Their effect was more significant in the kinetics than in the thermodynamics, which led to a delayed demixing in membrane formation and then, the formation of a long finger-like structure with macrovoids free. These changes could be explained by the following reasons: metal nanoparticles increased the thermodynamic instability of the polymer solution when reacted with

water, which could cause a rapid phase demixing and then, the macrovoid formation [11]. However, metal nanoparticles have higher affinity for water compared to PES material (especially metal oxides such as ZnO), resulting in a longer time for the exchange between the non-solvent in the coagulation bath and the solvent in the polymer casting film before gelation and vitrification. Therefore, when the casting solution was immersed in the coagulation bath, longer exchange between solvent and non-solvent led to form larger finger-like pores [45]. Also, these metal nanoparticles had strong interactions with PES/NMP, which was reflected in a significant increase in viscosity (data not shown) and was confirmed by other authors, who worked with incorporating nano-ZnO in PES structures [46,47]. These effects caused a delay in the precipitation of the polymer (a decrease in the diffusion rate of water into the polymer film) and then, the existing macrovoids in the synthesized membranes were partially suppressed due to the delayed liquid-liquid demixing [11,31].

For all these reasons, both types of nanoparticles have the same effect in the membrane structure. Albeit, the suppression of macrovoids in presence of hydrophilic ZnO nanoparticles was lower in comparison with PES membranes with hydrophobic WS_2 nanoparticles. The higher affinity of nano-sized ZnO for water molecules (compared to hydrophobic WS_2 nanoparticles) suppressed the diffusion of solvent through the polymer solution due to the competitive mass transfer between ZnO and solvent, which favoured the formation of a sponge-like structure in the sublayer and as a consequence, the presence of small macrovoids [48].

These results were corroborated with the cloud point measurements for PES/NMP/water (represented as PES membrane) and (PES + metal nanoparticles)/NMP/water systems

obtained by the visual titration method and presented in Fig. 2. It can be observed that the values obtained for PES/NMP/water system were consistent with the literature [8,44,49]. If each system formed by base polymer and metal nanoparticles is considered as a pseudo single component during the initial stages of the liquid-liquid phase separation, this quaternary system can be represented as a pseudo ternary diagram and in this way, it could be possible the study of the presence of different metal nanoparticle concentrations on the control system formed by polymer/solvent/non-solvent. Irrespective of the hydrophobicity of both metal nanoparticles, the changes in the phase border curves (binodal curves) is observed in the miscibility gap, where the critical point was moved far from the polymer-solvent axis in comparison with the system without nanoparticles and therefore, the homogeneous region was enlarged and more water was needed for the precipitation of PES in these (PES + metal nanoparticles)/NMP/water systems. Thus, the presence of metal nanoparticles could absorb more water molecules and then, the system presented larger tolerance to non-solvent. Furthermore, the shift of the binodal curves in PES/metal nanoparticles membranes in the cloud point measurements indicated the membrane development by a more delayed liquid-liquid demixing in comparison with the PES/NMP/water system, resulting in narrower, longer and denser finger-like structures without the presence of macrovoids (as it was shown in Fig. 1) [50].

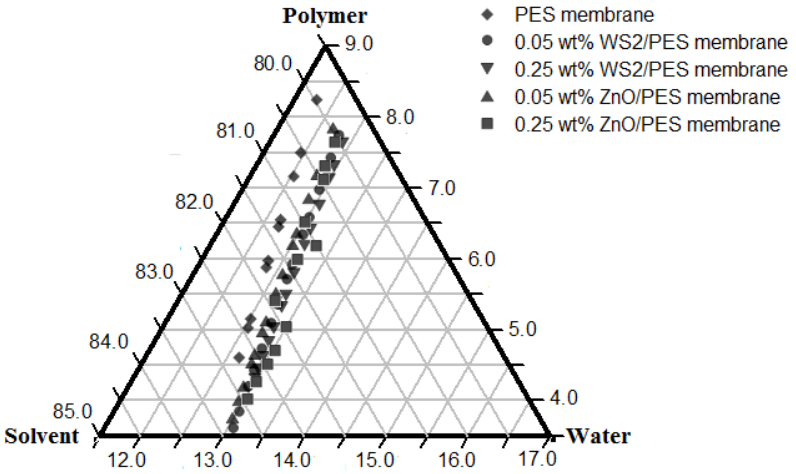

Fig. 2. Ternary phase diagram of PES with and without metal nanoparticles using NMP as solvent constructed based on cloud point measurements by titration method at 20 ºC.

In addition, some nanoparticles trapped inside the porous sublayer can be seen in the SEM images of the synthesised membranes, especially in membranes with high concentrations of nanoparticles (marked with red arrows) due to the low dispersion of the entrapped nanoparticles at these conditions and their agglomeration in the matrix structure (see Fig. 1). The agglomeration of nanoparticles plays a large role in improving effectively the membrane properties. The presence of agglomerations can be principally caused by the high surface energy of the metal nanoparticles, which tend to agglomerate for diminishing their surface energy to reach a more stable state. For this reason, these agglomerations lead to a bad distribution of metal nanoparticles along both polymer structure and surface, negatively altering membrane flux and antifouling properties by changing parameters such as surface roughness and hydrophilicity [47,51,52]. Some researchers suggested that the preparation of nanoparticles with a stabilizer and the use of ultrasonication could be applied in order to prevent the agglomeration of metal nanoparticles [53,54].

Simultaneously to SEM technique, EDX analysis was performed to corroborate the presence of the different metal nanoparticles on the surface structure (the active layer).

The compositions of metal nanoparticles were collected for five different samples and the average values are summarised in Table 1. The results demonstrated the presence of C, O and S for all the membranes (from the PES material) and the existence of metal nanoparticles in their corresponding membranes. When the WS_2 concentration increased in the casting solution, the presence of W and S elements in the surface structure also increased. In the case of ZnO/PES membranes, the same trend was observed where the content of Zn and O elements increased. Therefore, even if the values obtained were very small, the content of metal nanoparticles in each sample increased with its increment in the casting solution.

Table 1. EDX results for each synthesised membrane with and without metal nanoparticles by phase inversion method.

Membrane	**Element**				
	C	**S**	**O**	**W**	**Zn**
	wt%	**wt%**	**wt%**	**wt%**	**wt%**
PES	26.86 ± 0.93	2.57 ± 0.51	70.57 ± 0.67	0.00 ± 0.00	0.00 ± 0.00
0.05 wt% WS_2/PES	26.12 ± 0.49	3.74 ± 0.51	70.10 ± 0.91	0.04 ± 0.01	0.00 ± 0.00
0.25 wt% WS_2/PES	24.28 ± 1.02	5.54 ± 1.27	70.09 ± 1.61	0.09 ± 0.02	0.00 ± 0.00
0.05 wt% ZnO/PES	25.65 ± 0.99	2.90 ± 1.41	71.43 ± 0.46	0.00 ± 0.00	0.02 ± 0.01
0.25 wt% ZnO/PES	25.56 ± 0.96	2.91 ± 0.87	71.47 ± 0.95	0.00 ± 0.00	0.06 ± 0.02

In order to confirm the presence of these species on the membrane surface, FTIR-ATR analyses were performed for all the synthesised membranes. The FTIR-ATR spectra of the control PES membrane and all the (PES + metal nanoparticle) membranes are shown in Fig. 3. In this operating range of wavelengths, the spectra related to WS_2/PES membranes exhibited a similar FTIR-ATR spectrum to those obtained for PES membranes, except the 1151 cm^{-1} peak which was shifted to 1148 cm^{-1} and also, its intensity was slightly increased. These changes could be attributed to the presence of sulphur-containing groups and are in accordance with those obtained by other researchers [55]. In the case of PES membranes with ZnO nanoparticles, two new absorption bands appeared at 1660 cm^{-1} and at 3100-3600 cm^{-1} respectively, which

could be assigned to O-H groups of adsorbed water by hydrophilic nano-sized ZnO [56-58].

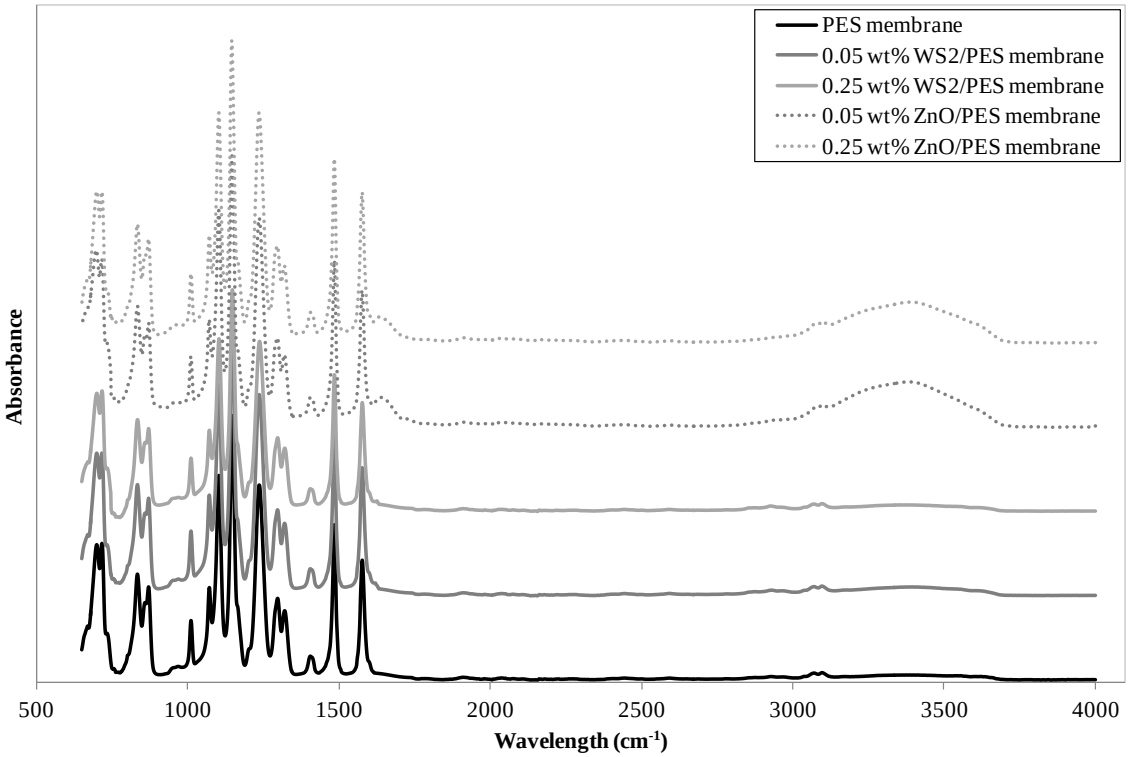

Fig. 3. FTIR-ATR spectra of all the membrane surfaces for different compositions of metal nanoparticles.

Fig. 4 provides the three-dimensional AFM images for all the synthesised membranes, both with and without metal nanoparticles. The brightest area presents the highest points of the sample surface and the dark regions illustrate valleys or sample pores. From the AFM images, it can be seen that bare PES membrane showed a smoother surface than (PES + metal nanoparticle) membranes. The presence of nanoparticles caused a surface with larger peaks and therefore, membrane roughness was increased. These results were numerically confirmed with the calculated roughness values for each membrane surface presented in Table 2. Although the roughness values were very similar in all the membranes and there were no significant differences among them, metal nanoparticles tend to protrude at PES membrane surface during immersion-precipitation method even in ultra-low concentrations and increased the roughness values. This behaviour was

observed by other researchers in previous studies [59]. In the same way, the presence of agglomerations could be observed in PES membranes with high concentration of metal nanoparticles, especially in 0.25 wt% ZnO/PES membranes. These agglomerations are represented in the AFM image as broad hills on the membrane surface, which led to an uneven distribution of nanoparticles on the surface structure. This could negatively affect the permselective properties of the membrane [52].

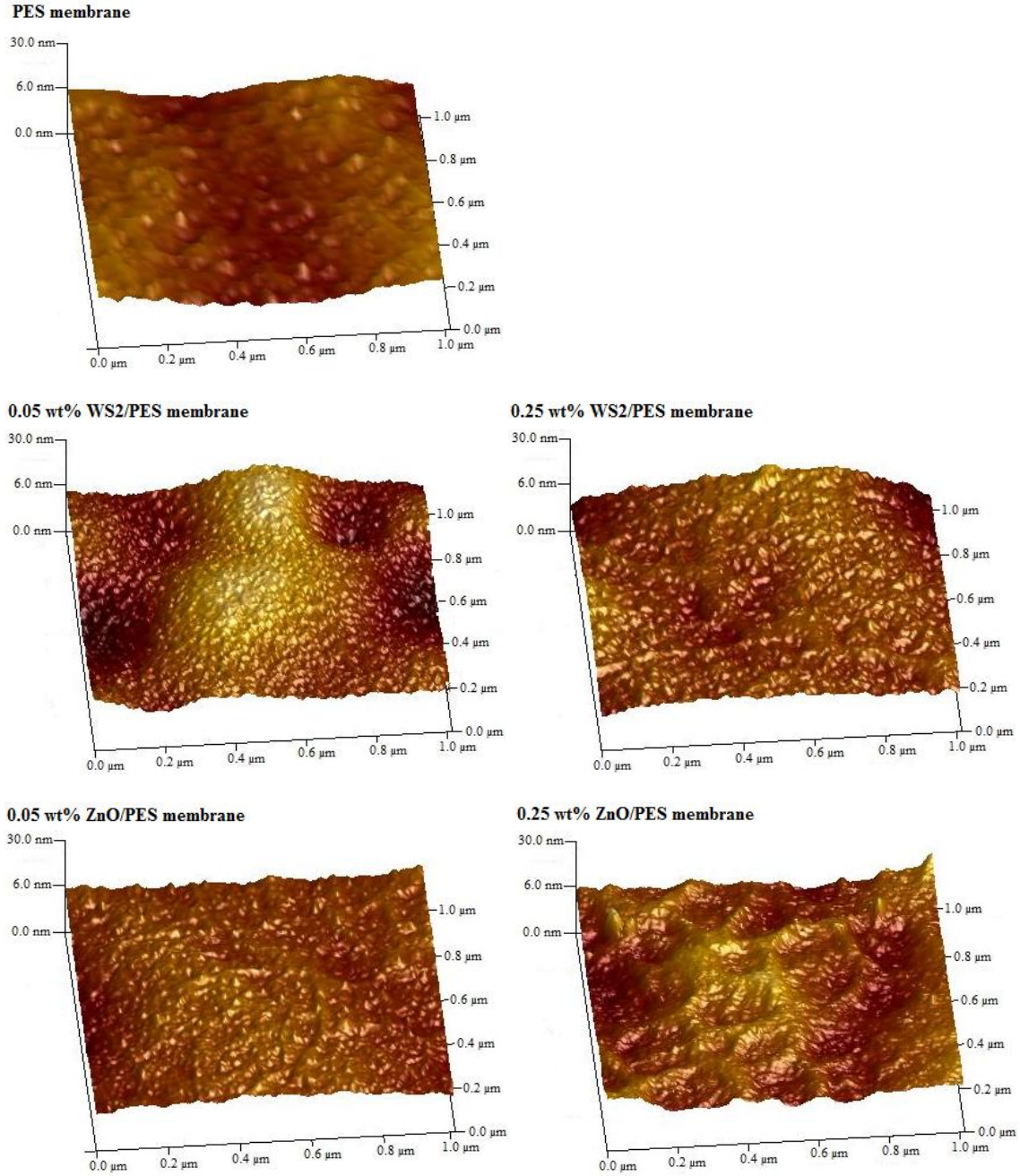

Fig. 4. Surface 3D AFM images of unmodified PES membrane and PES membranes modified with different concentrations of metal nanoparticles.

Table 2. Membrane resistance (R_m) and roughness parameters (S_a and S_q) for each synthesised membrane.

Membrane	R_m ($\cdot 10^{12}$ m^{-1})	S_a (nm)	S_q (nm)
PES	4.162 ± 0.107	3.9 ± 0.1	5.0 ± 0.2
0.05 wt% WS_2/PES	3.372 ± 0.106	4.4 ± 0.1	5.7 ± 0.3
0.25 wt% WS_2/PES	2.630 ± 0.083	5.4 ± 0.2	6.8 ± 0.4
0.05 wt% ZnO/PES	2.456 ± 0.094	4.3 ± 0.1	5.6 ± 0.2
0.25 wt% ZnO/PES	1.413 ± 0.056	4.7 ± 0.2	5.8 ± 0.2

Water contact angle measurements are the most commonly used parameter to describe the hydrophilic character of a membrane. Fig. 5 shows the water contact angle measurements for the different membranes prepared. The control membrane was the least hydrophilic, as it had a water contact angle of 77.1 ± 1.96º, which was the highest value obtained for water contact angle measurements among all the membranes tested. This value shows the semi-hydrophobic nature of PES and is in accordance with the studies of other researchers [37,38,60]. As can be observed in this figure, an increasing metal nanoparticles concentration caused a decline in the contact angle values of the different membranes, indicating an increase in the surface hydrophilicity due to the high affinity of nanoparticles for water compared to PES material. In the same way, the structural changes caused by adding metal nanoparticles may also have some influence in the contact angle results, which led to an increase in surface pore density and pore size (as will be explained in porosity and MWCO section). All these effects could cause an increase in water absorption and permeation. In addition to all these effects and due to its hydrophobic character, the improvement of the hydrophilicity in PES membranes with ultra-low WS_2 concentrations (0.05 wt% WS_2/PES ratio) could also be related the presence of small amounts of WO_3 in these WS_2 nanoparticles [28,61]. However, their predominant hydrophobic character appears when their concentration increased (0.25 wt% WS_2/PES ratio), which led to a slight increase in the contact angle values (70.1 ± 2.47º) next to those obtained for the bare PES membrane. The lowest contact angle

values were obtained for ZnO/PES membranes, which nano-sized ZnO presented higher hydrophilic character than WS_2 nanoparticles. These results were consistent with the high surface area of nano-ZnO and therefore, its ability to absorb hydrophilic hydroxyl groups because a larger fraction of water could pass through the membrane structure. Shen et al. demonstrated that the presence of ZnO nanoparticles on the PES surface and in its matrix structure generated two effects: an increase in the hydrophilicity and also, an increase in the viscosity, as it was observed during the preparation of the polymer solutions [46]. When the ZnO concentration increased in the membrane (from 0.05 to 0.25 wt% ZnO/PES ratio), contact angle did not change significantly which indicates that the presence of ultra-low concentrations of ZnO can notably improve the hydrophilicity of a membrane, as it has been confirmed in other studies [38,62].

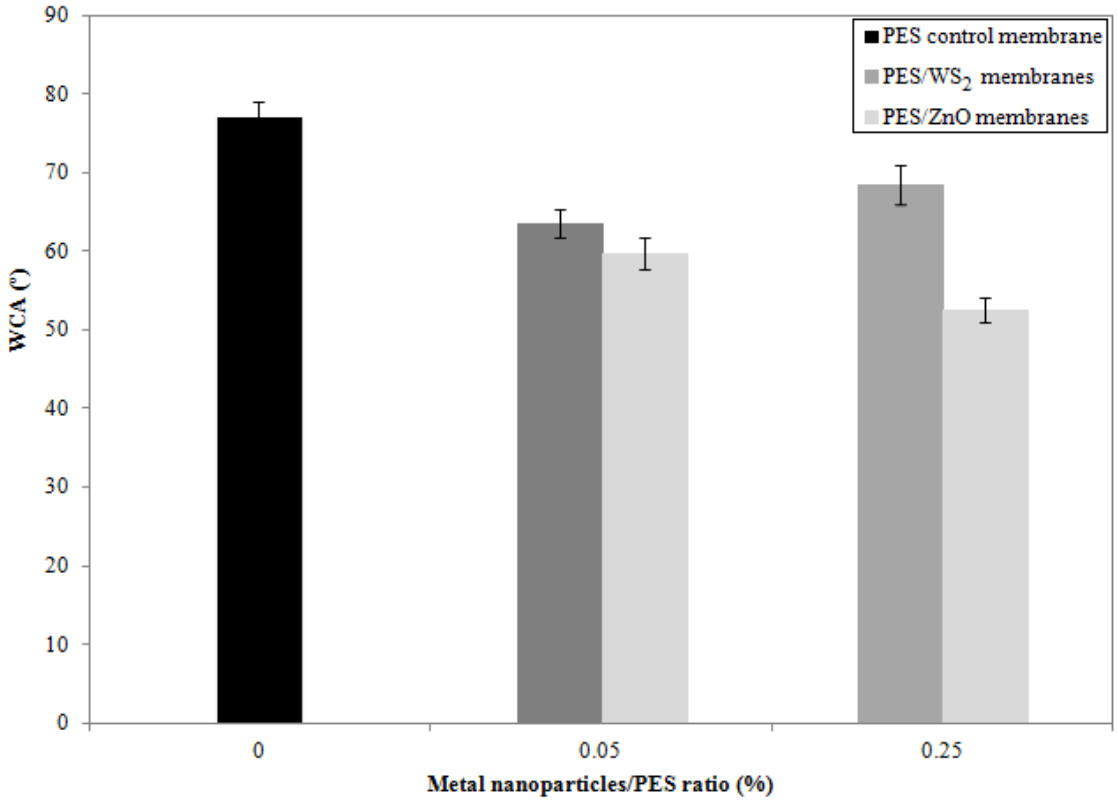

Fig. 5. Water contact angle (WCA) values measured for PES control membrane and PES/metal nanoparticles membranes at different metal nanoparticles/PES ratios.

Fig. 6 shows both plane and thickness shrinkage ratios obtained after the preparation of PES membranes with different metal nanoparticle content. During the phase separation, exchange of solvent and non-solvent takes place between the polymer solution film and the coagulation bath in which shrinkage occurs [63,64]. The polymer solution film shrinks in both the direction parallel (plane shrinkage ratio) and perpendicular (thickness shrinkage ratio) to the support. It can be observed in Fig. 6 that the plane shrinkage ratio is in a smaller scale than the thickness shrinkage ratio for all the synthesised membranes. These results are in accordance with the studies carried out by Finken, who demonstrated that a membrane cast on a backing material (non-woven support) could only shrink in thickness because lateral shrinkage is hindered by the strong bonding between membrane and support [65]. In the same way, lateral shrinkage (plane shrinkage ratio) decreased when the content of metal nanoparticle increased in the polymer solution, which could be caused by the change in viscosity of these solutions. This phenomenon opposes high resistance against lateral shrinkage because the interactions between the nonwoven support and the polymer solution with metal nanoparticles are strengthened [63]. However, thickness shrinkage increased with higher concentration of metal nanoparticle in PES solutions, especially in PES/ZnO membranes, which indicated that the mechanisms of both shrinkages (lateral and thickness shrinkage) have the same origin but their effects on the final dimensions of the membrane are different. Thickness shrinkage is the combination of the retraction of the polymer film during the casting process (before immersion) on the nonwoven support and the shrinkage caused by the precipitation of the polymer (during immersion) [63]. It can be observed that thickness shrinkage increased with the addition of metal nanoparticle due to the higher affinity of these nanoparticles for water molecules and their hindrance effect during the phase inversion process, which could

cause interfacial stresses between polymer and nanoparticles and then, an increase in membrane porosity due to the formation of interfacial pores by the shrinkage of organic phase during the demixing process [66]. The effect of thickness shrinkage on the membrane structure associated to the agglomeration of metal nanoparticles could induce the presence of macrovoids, which can be prevented by the addition of metal nanoparticles at ultra-low concentrations (see Fig. 1).

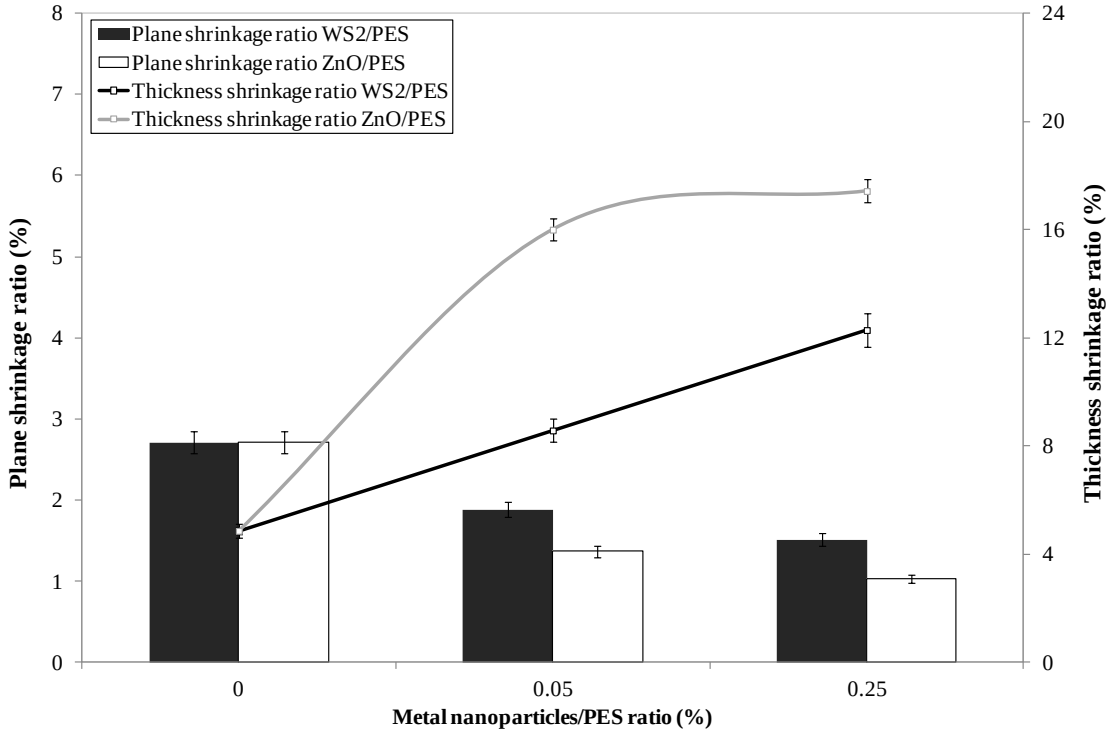

Fig. 6. Plane and thickness shrinkage ratios in PES membranes with different metal nanoparticle content.

Fig. 7 shows the change in the porosity before and after the presence of metal nanoparticles in the PES matrix structure of all the synthesised membranes. The incorporation of different types and concentrations of metal nanoparticles resulted in a slight increase in the overall porosity of the membrane [67], which could also be observed in SEM images because the number of fingers increased along the sublayer structure and also near to the surface. The difference between membranes with and without metal nanoparticles was remarkable after adding ultra-low contents of metal

nanoparticles, where the overall porosity increased from 51.0 ± 0.5 % for the bare PES membranes to 56.2 ± 0.5 % for 0.05 wt% ZnO/PES membranes. At high ZnO concentration, porosity increased up to 60.5 ± 0.6 %. Similar trends but lower increases were observed when WS_2 nanoparticles were added, obtaining an overall porosity of about 55 % for both WS_2/PES membranes. These results could be related to the higher values of surface roughness in membranes with metal nanoparticles and the decrease in their water contact angle results. Higher surface roughness caused higher porosity on the membrane surface and, combined with the lower contact angle values obtained, caused an improvement in hydrophilicity [68]. This improvement further confirmed the hydrophilicity of the membrane surface and pore walls with the introduction of nano-sized metal, especially with ZnO nanoparticles.

3.2. Filtration experiments

The effect of metal nanoparticles in the water permeability is shown in Fig. 7. In general, with increasing the concentration of metal nanoparticles, the water permeability increased. A strong correlation between the results obtained for both the membrane porosity and the water permeability was observed, which followed the same trend after incorporating the metal nanoparticles. When metal nanoparticles were added, a more porous membrane was formed and its skin layer could be reduced. This effect caused a decline in the intrinsic membrane resistance (see Table 2) and then, the increase of the water permeability. Thus, an increase in the membrane porosity is directly related to the increase in water permeability [61,68]. This phenomenon was remarkably reflected in membranes with ZnO nanoparticles in their composition (where the maximum permeability for water was observed at high ZnO concentration, 285.01 $L/m^2 \cdot h \cdot bar$), which can also be explained by the alteration of the membrane structure and the

improvement in the affinity of the modified polymeric matrix for water molecules caused by high hydrophilic character of these nanoparticles [38]. Furthermore, this increase in water permeability can be also related to the decrease in lateral shrinkage (plane shrinkage ratio) principally due to the presence of inorganic particles in the membrane structure as was reported by Aerts et al. [63].

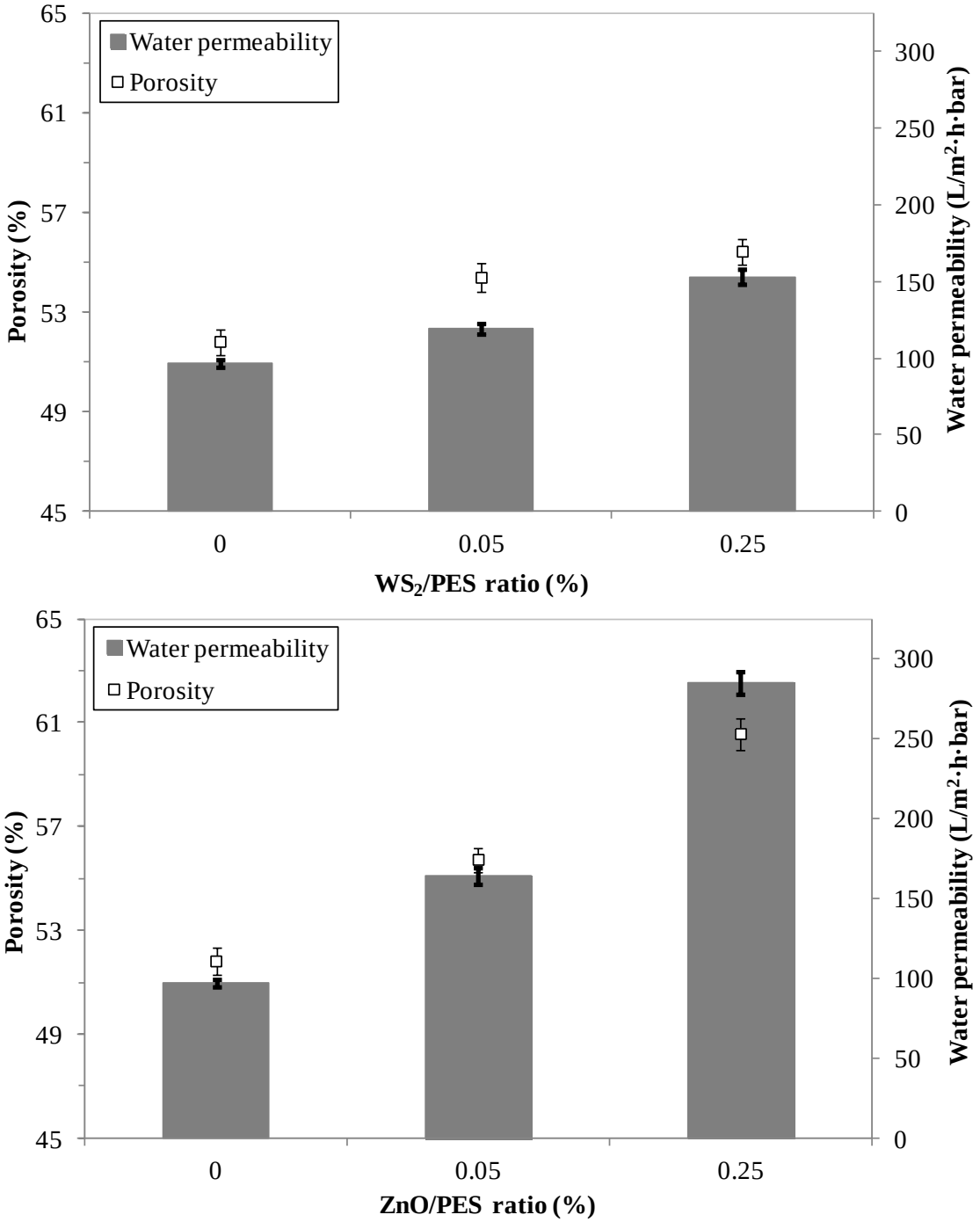

Fig. 7. Correlation between water permeability and porosity of the synthesised membranes.

MWCO measurements are widely used to determine the pore size of the membrane and this parameter can be defined as the molecular weight of the solute that has a rejection value of 90 %. The PEG separation curves used for measuring the MWCO of each membrane are depicted in Fig. 8. At the same conditions, all the synthesised membranes had a MWCO between 15 and 23 kDa (a solute radius between 3.67 and 4.50 nm, respectively), where the control PES membrane presented the lowest MWCO obtained. The incorporation of WS_2 nanoparticles in PES membranes had a small effect in the pore size, which increased up to 18 kDa (3.92 nm) at low concentrations and 20 kDa (4.16 nm) at high concentrations. However, the effect of nano-sized ZnO in pore size was higher, increasing this parameter up to 20 kDa (4.16 nm) at low concentrations and 23 kDa (4.50 nm) at high concentrations. Thus, even at ultra-low concentrations, a smaller increase in the content of metal nanoparticles slightly increased the pore size of the membrane. Although the addition of metal nanoparticles at ultra-low concentrations could cause the suppression of macrovoids inside the membrane structure, the smaller increase in the overall porosity, pore density (as it was observed in SEM images) and surface roughness had a predominant role on the membrane performance, which led to an increase in pore size in the same range. This strong relationship was also observed by other researchers [36].

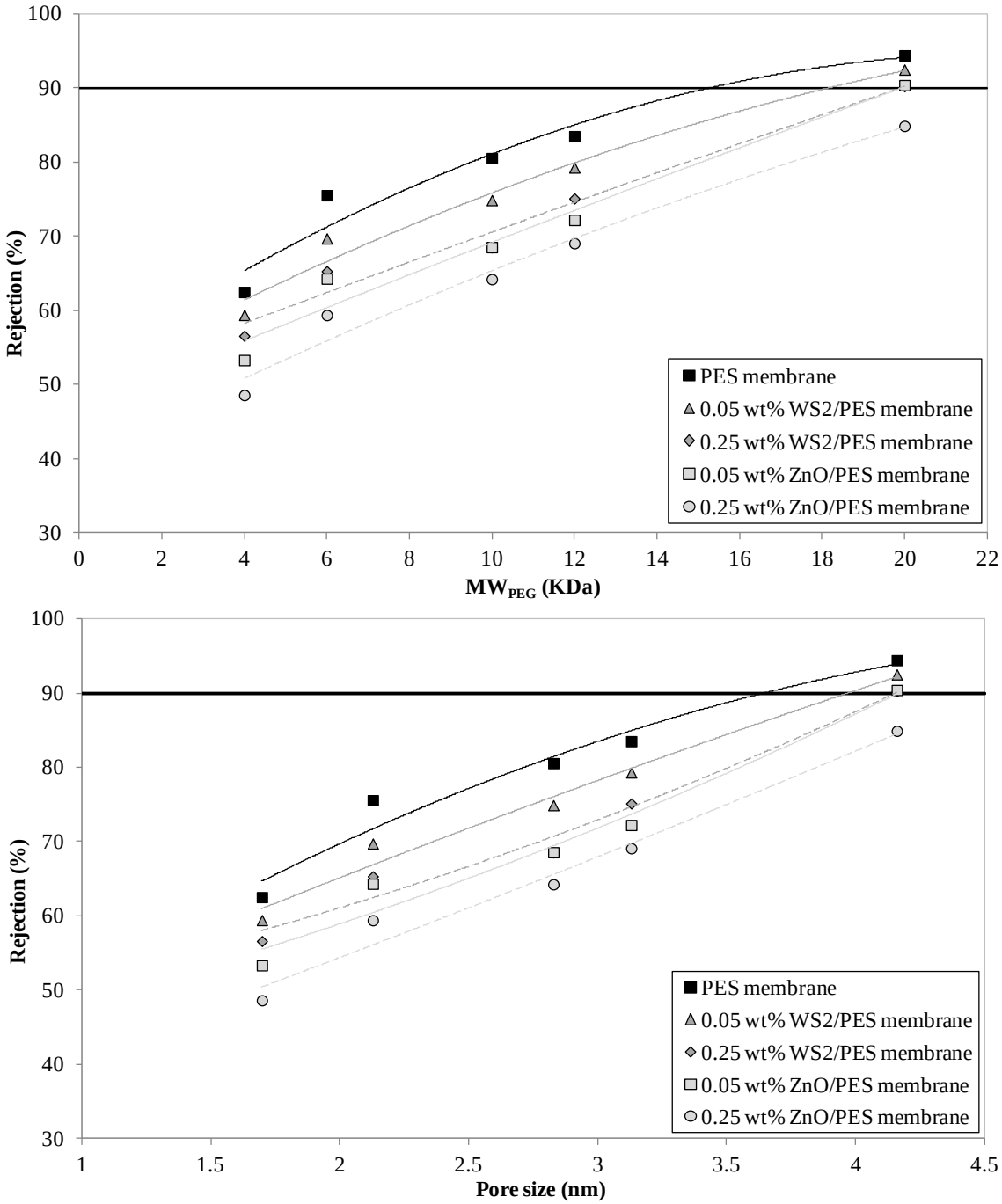

Fig. 8. MWCO measurement of membranes with and without metal nanoparticles in their structure using different PEG solutions at a concentration of 1 g/L.

The rejection values of HA solutions with each synthesised membrane are shown in Fig. 9. The rejection coefficients for the modified membranes are higher than that obtained for the control PES membrane, which implied an enhancement in HA rejection due to the incorporation of metal nanoparticles into the membrane structure and on its surface. This improvement could be better observed in PES membranes with ultra-low contents

of metal nanoparticles, due to the better dispersion of the metal nanoparticles at these conditions in comparison with the worse dispersion and formed agglomerations at high content of nanoparticles.

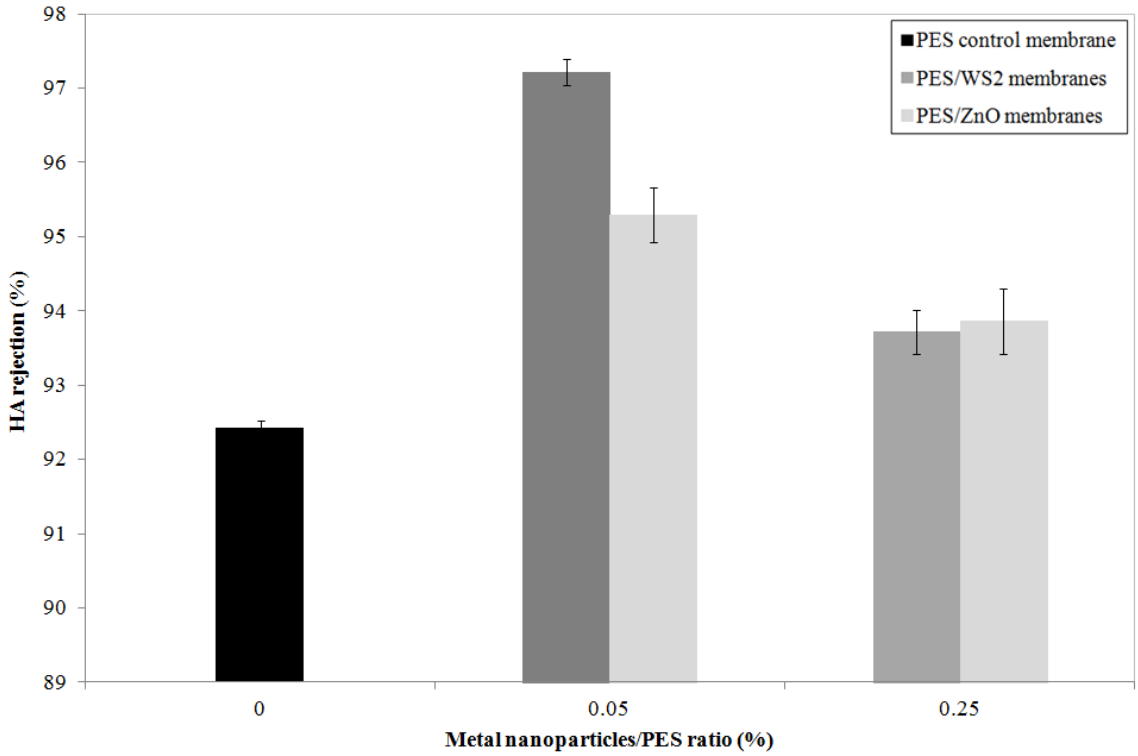

Fig. 9. Rejection performances at different metal nanoparticles concentrations using HA solutions at a concentration of 500 mg/L.

Fig. 10 shows the normalised flux ratio (NFR) as a function of time during the constant pressure (2 bar) filtration of HA solutions through each synthesised membrane. The WS_2/PES membrane with the highest WS_2 content exhibited the highest flux decline (~ 37 % of NFR), which was very similar to the control PES membrane (~ 40 % of NFR). At high WS_2 concentration, the hydrophobic character of the combination WS_2/PES (as it was depicted in Fig. 5) played a dominant role in the membrane permselectivity and made the membrane more susceptible to fouling. Nevertheless, the PES membrane with the lowest ZnO content exhibited the lowest flux decline (~ 50 % of NFR) followed by the 0.05 wt% WS_2/PES membrane (~ 48 % of NFR). These results are an indicator that the potential application of ultra-low contents of nanoparticles (irrespective to their

nature) to improve the membrane performance and its antifouling properties, because the presence of metal nanoparticles at ultra-low concentrations reduced the hydrophobic interactions between the PES membrane and the foulant HA [38,61]. This is in accordance with the water contact angle results described above. It is well known that the improvement of the membrane surface hydrophilicity inhibits the existing interactions between solute (organic matter) and membrane surface, which avoids the undesired fouling phenomena [61,69]. However, the effect of high concentrations of metal nanoparticles in membrane performance could be related to the increase in pore size, porosity and roughness, which led to a higher flux decline and a less selective membrane compared to membranes with ultralow content of metal nanoparticles.

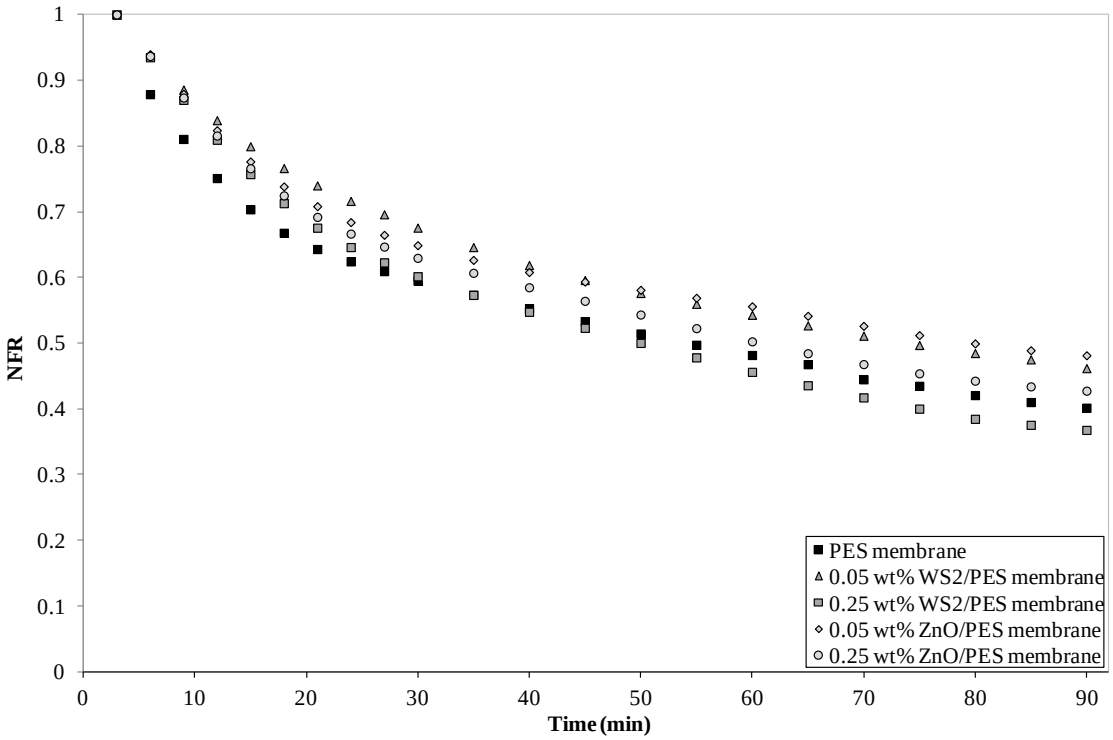

Fig. 10. Normalised flux ratio (NFR) of PES membranes with and without metal nanoparticles using HA solutions at a concentration of 500 mg/L. T = 25 ºC and ΔP = 2 bar.

4. CONCLUSIONS

In order to determine the influence on the structure formation, intrinsic characteristics and permselective properties of a MMM prepared by NIPS method, the incorporation of

nanoparticles at ultra-low concentrations in the polymer casting solution was studied. For this purpose, two metal nanoparticles of opposite hydrophobicity and characteristics (hydrophilic ZnO and hydrophobic WS_2) at two different concentrations were compared (0.05 and 0.25 wt% metal nanoparticle/PES ratio). Irrespective of the hydrophobicity of both metal nanoparticles, modified membranes showed a structural change from a channel-like structure with the presence of macrovoids to a finger-like structure with the partial or total suppression of the macrovoids (the former in the case of ZnO/PES membranes and the latter in the case of WS_2/PES membranes), where this delay in the liquid-liquid demixing was confirmed by SEM analysis and cloud point measurements. At high concentrations of metal nanoparticles, the presence of agglomerations in the sublayer structure was observed. FTIR-ATR, EDX and AFM results demonstrated the presence of both species in the surface of the different synthesised membranes, increasing the surface roughness as well as the overall porosity of the membrane. Even at ultra-low concentrations, this last parameter (overall porosity) presented a strong relationship with the pore size and water permeability in both control and modified membranes, especially for ZnO/PES membranes where the increment was more significant. Contact angle results corroborated the improvement in the membrane hydrophilicity using both metal nanoparticles at low concentrations, which can be explained by the higher affinity of both inorganic compounds for water in comparison with the base PES material, especially for hydrophilic ZnO nanoparticles. The possible presence of WO_3 on the nano-sized WS_2 can provide more hydrophilic character to these nanoparticles. Furthermore, the addition of ultra-low concentrations of metal nanoparticles in the membrane structure significantly improved both HA rejection and antifouling properties, which confirms the improvement of the membrane hydrophilicity. Therefore, regardless of their hydrophilicity, the presence of metal

nanoparticles at ultra-low concentrations can cause similar structural changes when they were added in a polymeric matrix structure.

5. REFERENCES

[1] R.M. Boom, Th. Van den Boomgaard, C.A. Smolders, Mass transfer and thermodynamics during immersion precipitation for a two-polymer system. Evaluation with the system PES-PVP-NMP-water, J. Membr. Sci. 90 (1994) 231-249.

[2] M. Mulder. Basic Principles of Membrane Technology, Kluwer Academic Publishers, Dordrecht, The Netherlands, 2003.

[3] G.R. Guillen, Y. Pan, M. Li, E.M.V. Hoek, Preparation and characterization of membranes formed by nonsolvent induced phase separation: a review, Ind. Eng. Chem. Res. 50 (2011) 3798-3817.

[4] A.J. Reuvers, J.W.A. Van den Berg, C.A. Smolders, Formation of membranes by means of immersion precipitation. Part I. A model to describe mass transfer during immersion precipitation, J. Membr. Sci. 34 (1987) 45-65.

[5] A.J. Reuvers, C.A. Smolders, Formation of membranes by means of immersion precipitation. Part II. The mechanism of formation of membranes prepared from the system CA/acetone/water, J. Membr. Sci. 34 (1987) 67-86.

[6] C.A. Smolders, A.J. Reuvers, R.M. Boom, I.M. Wienk, Microstructures in phase-inversion membranes. Part 1. Formation of macrovoids, J. Membr. Sci. 73 (1992) 259-275.

[7] M. Di Luccio, R. Nobrega, C.P. Borges, Microporous anisotropic phase inversion membranes from bisphenol-A polycarbonate: study of a ternary system, Polymer 41 (2000) 4309-4315.

[8] W.W.Y. Lau, M.D. Guiver, T. Matsuura, Phase separation in polysulfone/solvent/water and polyethersulfone/solvent/water systems, J. Membr. Sci. 59 (1991) 219-227.

[9] M. Rezaei, A.F. Ismail, G. Bakeri, S.A. Hashemifard, T. Matsuura, Effect of general montmorillonite and Cloisite 15A on structural parameters and performance of mixed matrix membranes contactor for CO_2 absorption, Chem. Eng. J. 260 (2015) 875-885.

[10] D.M. Wang, J.Y. Lai, Recent advances in preparation and morphology control of polymeric membranes formed by nonsolvent induced phase separation, Curr. Opin. Chem. Eng. 2 (2013), 229-237.

[11] V. Vatanpour, S.S. Madaeni, L. Rajabi, S. Zinadini, A.A. Derakhshan, Boehmite nanoparticles as a new nanofiller for preparation of antifouling mixed matrix membranes, J. Membr. Sci. 401-402 (2012) 132-143.

[12] A.L. Ahmad, A.A: Abdulkarim, B.S. Ooi, S. Ismail, Recent development in additives modifications of polyethersulfone membrane for flux enhancement, Chem. Eng. J. 223 (2013) 246-257.

[13] C. Zhao, J. Xue, F. Ran, S. Sun, Modification of polyethersulfone membranes – a review of methods, Prog. Mater. Sci. 58 (2013) 76-150.

[14] M.A. Zarbin, C. Montemagno, J.F. Leary, R. Ritch, Nanotechnology in ophthalmology, Can. J. Ophthalmology 45 (2010) 457-476.

[15] N.S. Santos-Magalhães, V.C. Furtado-Mosqueira, Nanotechnology applied to the treatment of malaria, Adv. Drug Delivery Rev. 62 (2010) 560-575.

[16] C.M. Costa, J.L. Gomez Ribelles, S. Lanceros-Méndez, G.B. Appetecchi, B. Scrosati, Poly(vinylidene fluoride)-based, co-polymer separator electrolyte membranes for lithium-ion battery systems, J. Power Sources 245 (2014) 779-786.

[17] C. Chellaram, G. Murugaboopathi, A.A. John, R. Sivakumar, S. Ganesan, S. Krithika, G. Priya, Significance of Nanotechnology in Food Industry, APCBEE Procedia 8 (2014) 109-113.

[18] A.D. Kiadeni, A. Rahimpour, M. Jahanshahi, A.A. Ghoreyshi, Novel carbon nano-fibers (CNF)/polysulfone (PSf) mixed matrix membranes for gas separation, J. Ind. Eng. Chem. 22 (2015) 199-207.

[19] S.M. Hosseini, S. Rafiei, A.R. Hamidi, A.R. Moghadassi, S.S. Madaeni, Preparation and electrochemical characterization of mixed matrix heterogeneous cation exchange membranes filled with zeolite nanoparticles: ionic transport property in desalination, Desalination 351 (2014) 138-144.

[20] H. Basri, A.F. Ismail, M. Aziz, Microstructure and anti-adhesion properties of PES/TAP/Ag hybrid ultrafiltration membrane, Desalination 287 (2012) 71-77.

[21] M.M. Khan, V. Filiz, G. Bengtson, S. Shishatskiy, M.M. Rahman, J. Lillepaerg, V. Abetz, Enhanced gas permeability by fabricating mixed matrix membranes of functionalized multiwalled carbon nanotubes and polymers of intrinsic microporosity (PIM), J. Membr. Sci. 436 (2013) 109-120.

[22] L.Y. Ng, A.W. Mohammad, C.P. Leo, N. Hilal, Polymeric membranes incorporated with metal/metal oxide nanoparticles: a comprehensive review, Desalination 308 (2013) 15-33.

[23] T.S. Chung, S.S. Chan, R. Wang, Z. Lu, C. He, Characterization of permeability and sorption in Matrimid/C60 mixed matrix membranes, J. Membr. Sci. 211 (2003) 91-99.

[24] C.P. Leo, W.P. Cathie Lee, A.L. Ahmad, A.W. Mohammad, Polysulfone membranes blended with ZnO nanoparticles for reducing fouling by oleic acid, Sep. Purif. Technol. 89 (2012) 51-56.

[25] J. Hong, Y. He, Polyvinylidene fluoride ultrafiltration membrane blended with nano-ZnO particle for photo-catalysis self-cleaning, Desalination 332 (2014) 67-75.

[26] X. Hou, P.T. Deem, K.L. Choy, Hydrophobicity study of polytetrafluoroethylene nanocomposite films, Thin Solid Films 520 (2012) 4916-4920.

[27] D. James, T. Zubkov, Photocatalytic properties of free and oxide-supported MoS_2 and WS_2 nanoparticles synthesized without surfactants, J. Photoch. Photobio. A 262 (2013) 45-51.

[28] H.A. Therese, J. Li, U. Kolb, W. Tremel, Facile large scale synthesis of WS_2 nanotubes from WO_3 nanorods prepared by a hydrothermal route, Solid State Sci. 7 (2005) 67-72.

[29] A. Costa, M.N. de Pinho, Effect of membrane pore size and solution chemistry on the ultrafiltration of humic substances solutions, J. Membr. Sci. 255 (2005) 49-56.

[30] F.S. Dehkordi, M. Pakizeh, M. Namvar-Mahboub, Properties and ultrafiltration efficiency of cellulose acetate/organically modified Mt (CA/OMMt) nanocomposite membrane for humic acid removal, Appl. Clay Sci. 105-106 (2015) 178-185.

[31] B.S. Lalia, V. Kochkodan, R. Hashaikeh, N. Hilal, A review on membrane fabrication: structure, properties and performance relationship, Desalination 326 (2013) 77-85.

[32] S. Darvishmanesh, J.C. Jansen, F. Tasselli, E. Tocci, P. Luis, J. Degrève, E. Drioli, B. Van der Bruggen, Novel polyphenylsulfone membrane for potential use in solvent nanofiltration, J. Membr. Sci. 379 (2011) 60-68.

[33] F. Luo, J. Zhang, X.L. Wang, J.F. Cheng, Z.J. Xu, Formation of hydrophilic EAA copolymer microporous membranes via thermally induced phase separation, Acta Polym. Sin. (2002) 566-571.

[34] L. Vikingsoon, B. Claessens, J.A. Gómez-Tejedor, G. Gallego-Ferrer, J.L. Gómez-Ribelles, Relationship between micro-porosity, water permeability and mechanical behaviour in scaffolds for cartilage engineering, J. Mech. Behav. Biomed. 48 (2015) 60-69.

[35] R. Rohani, M. Hyland, D. Patterson, A refined one-filtration method for aqueous based nanofiltration and ultrafiltration membrane molecular weight cut-off determination using polyethylene glycols, J. Membr. Sci. 382 (2011) 278-290.

[36] A. Idris, N.M. Zain, N.Y. Noordin, Synthesis, characterization and performance of asymmetric polyethersulfone (PES) ultrafiltration membranes with polyethylene glycol of different molecular weights as additives, Desalination 207 (2007) 324-339.

[37] J. Garcia-Ivars, M.I. Alcaina-Miranda, M.I. Iborra-Clar, J.A. Mendoza-Roca, L. Pastor-Alcañiz, Enhancement in hydrophilicity of different polymer phase-inversion ultrafiltration membranes by introducing PEG/Al_2O_3 nanoparticles, Sep. Purif. Technol. 128 (2014) 45-57.

[38] S. Balta, A. Sotto, P. Luis, L. Benea, B. Van der Bruggen, J. Kim, A new outlook on membrane enhancement with nanoparticles: the alternative of ZnO, J. Membr. Sci. 389 (2012) 155-161.

[39] S. Singh, K.C. Khulbe, T. Matsuura, P. Ramamurthy, Membrane characterization by solute transport and atomic force microscopy, J. Membr. Sci. 142 (1998) 111-127.

[40] R.W. Baker, Membrane Technology and Applications, second edition, John Wiley & Sons Ltd., Chichester, 2004.

[41] M. Meireles, A. Bessieres, I. Rogissart, P. Aimar, V. Sanchez, An appropriate molecular size parameter for porous membranes calibration, J. Membr. Sci. 103 (1995) 105-115.

[42] D.B. Mosqueda-Jimenez, R.M. Narbaitz, T. Matsuura, G. Chowdhury, G. Pleizier, J.P. Santerre, Influence of processing conditions on the properties of ultrafiltration membranes, J. Membr. Sci. 231 (2004) 209-224.

[43] M. Shaban, H. Abdallah, L. Said, H.S. Hamdy, A.A. Khalek, Titanium dioxide nanotubes embedded mixed matrix PES membranes characterization and membrane performance, Chem. Eng. Res. Des. 95 (2015) 307-316.

[44] J. Barzin, B. Sadatnia, Correlation between macrovoid formation and the ternary phase diagram for polyethersulfone membranes prepared from two nearly similar solvents, J. Membr. Sci. 325 (2008) 92-97.

[45] A. Rahimpour, S.S. Madaeni, A.H. Taheri, Y. Mansourpanah, Coupling TiO2 nanoparticles with UV irradiation for modification of polyethersulfone ultrafiltration membranes, J. Membr. Sci. 313 (2008) 158-169.

[46] L. Shen, X. Bian, X. Lu, L. Shi, Z. Liu, L. Chen, Z. Hou, K. Fan, Preparation and characterization of ZnO/polyethersulfone (PES) hybrid membranes, Desalination 293 (2012) 21-29.

[47] S. Zhao, W. Yan, M. Shi, Z. Wang, J. Wang, S. Wang, Improving permeability and antifouling performance of polyethersulfone ultrafiltration membrane by incorporation of ZnO-DMF dispersion containing nano-ZnO and polyvinylpyrrolidone, J. Membr. Sci. 478 (2015) 105-116.

[48] J. Lin, W. Ye, K. Zhong, J. Shen, N. Jullok, A. Sotto, B. Van der Bruggen, Enhancement of polyethersulfone (PES) membrane doped by monodisperse Stöber silica for water treatment, Chem. Eng. Process. (2015), http://dx.doi.org/10.1016/j.cep.2015.03.011

[49] L. Xu, F. Qiu, Simultaneous determination of three Flory-Huggins interaction parameters in polymer/solvent/nonsolvent systems by viscosity and cloud point measurements, Polymer 55 (2014) 6795-6802.

[50] M. Sadrzadeh, S. Bhattacharjee, Rational design of phase inversion membranes by tailoring thermodynamics and kinetics of casting solution using polymer additives, J. Membr. Sci. 441 (2013) 31-44.

[51] L.Y. Yu, H.M. Shen, Z.L. Xu, PVDF-TiO_2 composite hollow fiber ultrafiltration membranes prepared by TiO_2 sol-gel method and blending method, J. Appl. Polym. Sci. 113 (2009) 1763-1772.

[52] A. Razmjou, J. Mansouri, V. Chen, The effects of mechanical and chemical modification of TiO_2 nanoparticles on the surface chemistry, structure and fouling performance of PES ultrafiltration membranes, J. Membr. Sci. 378 (2011) 73-84.

[53] N. Mandzy, E. Grulke, T. Druffel, Breakage of TiO_2 agglomerates in electrostatically stabilized aqueous dispersions, Powder Technol. 160 (2005) 121-126.

[54] N.H.H. Hairom, A.W. Mohammad, A.A.H. Kadhum, Influence of zinc oxide nanoparticles in the nanofiltration of hazardous Congo red dyes, Chem. Eng. J. 260 (2015) 907-915.

[55] X. Hou, C.X. Shan, K.L. Choy, Microstructures and tribological properties of PEEK-based nanocomposite coatings incorporating inorganic fullerene-like nanoparticles, Surf. Coat. Tech. 202 (2008) 2287-2291.

[56] X. Zhang, Y. Wang, Y Liu, J. Xu, Y. Han, X. Xu, Preparation, performances of PVDF/ZnO hybrid membranes and their applications in the removal of copper ions, Appl. Surf. Sci. 316 (2014) 333-340.

[57] F. Parvizian, S.M. Hosseini, A.R. Hamidi, S.S. Madaeni, A.R. Moghadassi, Electrochemical characterization of mixed matrix nanocomposite ion exchange

membrane modified by ZnO nanoparticles at different electrolyte conditions "pH/concentration", J. Taiwan Inst. Chem. E. 45 (2014) 2878-2887.

[58] M.H. Farzana, S. Meenakshi, Visible light-driven photoactivity of zinc oxide impregnated chitosan beads for the detoxification of textile dyes, Appl. Catal. A-Gen (2014), http://dx.doi.org/10.1016/j.apcata.2014.12.034

[59] M. Sile-Yuksel, B. Tas, D.Y. Koseoglu-Imer, I. Koyuncu, Effect of silver nanoparticle (AgNP) location in nanocomposite membrane matrix fabricated with different polymer type on antibacterial mechanism, Desalination 347 (2014) 120-130.

[60] H. Susanto, M. Ulbricht, Photografted thin polymer hydrogel layers on PES ultrafiltration membranes: characterization, stability, and influence on separation performance, Langmuir 23 (2007) 7818-7830.

[61] J. Lin, R. Zhang, W. Ye, N. Jullok, A. Sotto, B. Van der Bruggen, Nano-WS_2 embedded PES membrane with improved fouling and permselectivity, J. Colloid Interf. Sci. 396 (2013) 120-128.

[62] Y. Jafarzadeh, R. Yegani, M. Sedaghat, Preparation, characterization and fouling analysis of ZnO/polyethylene hybrid membranes for collagen separation, Chem. Eng. Res. Des. 94 (2015) 417-427.

[63] P. Aerts, I. Genné, R. Leysen, P.A. Jacobs, I.F.J. Vankelecom, The role of the nature of the casting substrate on the properties of membranes prepared via immersion precipitation, J. Membr. Sci. 283 (2006) 320-327.

[64] M. Bikel, I.G.M. Pünt, R.G.H. Lammertink, M. Wessling, Shrinkage effects during polymer phase separation on microfabricated molds, J. Membr. Sci. 347 (2010) 141-149.

[65] H. Finken, Bentonite-stabilized CDA/CTA membranes. I. Improved long-term transport properties, Desalination 48 (1983) 207-221.

[66] A. Sotto, A. Boromand, R. Zhang, P. Luis, J.M. Arsuaga, J. Kim, B. Van der Bruggen, Effect of nanoparticle aggregation at low concentrations of TiO_2 on the hydrophilicity, morphology, and fouling resistance of PES-TiO_2 membranes, J. Colloid Interf. Sci. 363 (2011) 540-550.

[67] Y. Ma, F. Shi, Z. Wang, M. Wu, J. Ma, C. Gao, Preparation and characterization of PSf/clay nanocomposite membranes with PEG 400 as a pore forming additive, Desalination 286 (2012) 131-137.

[68] A. Ananth, G. Arthanareeswaran, H. Wang, The influence of tetraethylorthosilicate and polyethyleneimine on the performance of polyethersulfone membranes, Desalination 287 (2012) 61-70.

[69] J.H. Li, B.F. Yan, X.S. Shao, S.S. Wang, H.Y. Tian, Q:Q. Zhang, Influence of Ag/TiO_2 nanoparticle on the surface hydrophilicity and visible-light response activity of polyvinylidene fluoride membrane, Appl. Surf. Sci. 324 (2015) 82-89.

6. LIST OF SYMBOLS

Variables

A_m	Effective area of the membrane (m^2)
a_{after}	Length of the membrane sample after the casting process (cm)
$a_{theoretical}$	Length of the membrane sample before the casting process (cm)
$ab_{shrinkage}$	Plane shrinkage ratio (%)
b_{after}	Width of the membrane sample after the casting process (cm)
$b_{theoretical}$	Width of the membrane sample before the casting process (cm)
C_f	Solute concentration in the feed stream (mg/L)
C_p	Solute concentration in the permeate stream (mg/L)
D_{AB}	Diffusivity of solute (cm^2/s)

h_{after}	Thickness of the membrane sample after the casting process (μm)
$h_{shrinkage}$	Thickness shrinkage ratio (%)
$h_{theoretical}$	Thickness of the membrane sample before the casting process (μm)
J_0	Pure water flux at the end of compaction test (L/m^2·h)
J_f	Permeate flux during the filtration process (L/m^2·h)
J_{f1}	Permeate flux obtained at the beginning of the filtration process (L/m^2·h)
J_{f2}	Permeate flux at the end of the filtration process (L/m^2·h)
J_W	Permeate water flux (L/m^2·h)
k	Boltzmann's constant (dimensionless)
K_W	Hydraulic permeability (L/m^2·h·bar)
M_W	Molecular weight (Da)
NFR	Normalised flux ratio (%)
N_p	Number of points within the given area (dimensionless)
r	Stokes-Einstein radius (cm)
R	Solute rejection (%)
R_m	Membrane intrinsic resistance (m^{-1})
S_a	Average roughness (nm)
S_q	Root mean square roughness (nm)
t	Experimental time interval (h)
T	Temperature (°C)
V	Total volume permeated during an experimental time interval (L)
W_D	Weight of dry membranes (g)
W_W	Weight of wet membranes (g)
Z	Height values of the surface sample (nm)
Z_{avg}	Average of the Z values of the sample (nm)

Z_i	Z value currently measured (nm)

Greek letters

[η]	Intrinsic viscosity of PEG (dl/g)
ΔP	Transmembrane pressure (MPa)
ε	Membrane porosity (%)
η	Solvent (water) viscosity (N s/m^2)
μ	Dynamic water viscosity (Pa s)
ρ_p	Density of the polymer (g cm^{-3})
ρ_W	Density of pure water at operating conditions (g cm^{-3})

Abbreviations

AFM	Atomic force microscopy
EDX	Energy dispersive X-ray spectroscopy
FTIR-ATR	Fourier transform IR spectroscopy with attenuated total reflectance
HA	Humic acid
MMMs	Mixed matrix membranes
MWCO	Molecular weight cut-off
NIPS	Non-solvent induced phase separation
NMP	N-methyl-2-pyrrolidone
NOM	Natural organic matter
PEG	Polyethylene glycol
PES	Polyethersulphone
SEM	Scanning electron microscopy
UV	Ultraviolet